Energy & Environmental Science

Accepted Manuscript

ROYAL SOCIETY OF CHEMISTRY

www.rsc.org/ees

High-Performance p-Cu_2O/n-TaON Heterojunction Nanorod Photoanodes Passivated with Ultrathin Carbon Sheath for Photoelectrochemical Water Splitting

Jungang Hou,[ab] Chao Yang,[a] Huijie Cheng,[a] Shuqiang Jiao,[a] Osamu Takeda,[b] Hongmin Zhu[ab*]

[a]School of Metallurgical and Ecological Engineering, University of Science and Technology Beijing, Beijing 100083, China

[b]Tohoku University, 6-6-02 Aramaki-Aza-Aoba, Aoba-ku, Sendai, 980-8579 Japan

Corresponding author: hzhu@material.tohoku.ac.jp

Abstract:

Considerable efforts have been made to design and discover photoactive nanostructured (oxy)nitride materials that can be used as photoanodes for photoelectrochemical (PEC) water splitting. However, the high recombination rate of photoexcited electron–hole pairs and the poor photostability greatly limited their practical applications. Herein, the p-type Cu_2O/n-type TaON heterojunction nanorod array passivated with ultrathin carbon sheath (carbon–Cu_2O/TaON) as a surface protection layer was achieved via a solution-based process. Due to the shape anisotropy and p-n heterojunction structure, the photocurrent density of carbon–Cu_2O/TaON heterojunction nanorod arrays as the integrated photoanode with a maximum IPCE of 59% at 400 nm, reached 3.06 mA cm^{-2} under AM 1.5G simulated sunlight at 1.0 V vs. RHE and remained at about 87.3 % of the initial activity after 60 min irradiation, exhibiting that not only the onset potential is negatively shifted but also the photocurrent and photostability are significantly improved in comparison to that

of TaON and Cu_2O/TaON due to a high built-in potential in the protective p–n heterojunction device encapsulated in an ultrathin graphitic carbon sheath from the electrolyte. Our design introduces material components to provide a dedicated charge-transport pathway, alleviating the reliance on the materials' intrinsic properties, and therefore has the potential to greatly broaden where and how various existing materials can be used in energy-related applications.

KEYWORDS: TaON nanorod arrays; Cu_2O nanoparticles; ultrathin carbon sheath; heterojunction engineering; photoelectrochemical water splitting

1. Introduction

Photoelectrochemical (PEC) water splitting offers the capability of harvesting the energy in solar radiation and transferring it directly to chemical bonds for easy storage, transport, and use in the form of hydrogen.[1-3] Among the various efforts of a PEC system, the appropriate choice of photoelectrode materials using solar energy is especially important because their properties, such as optical absorption characteristics and chemical stability, determine the system's performance.[1-2] Most metal oxides, such as Fe_2O_3,[4,5] TiO_2,[6,7] WO_3[8,9] and $BiVO_4$[10-12] have received immense attention as photoelectrodes for PEC conversion of solar energy into chemical fuels. However, compared to that of the oxygen 2p orbital, different (oxy)nitrides with narrow band gap could potentially encompass nearly the larger solar spectrum due to the more negative potential of the nitrogen 2p orbital.[13]

Among these (oxy)nitrides containing Ta^{5+} or Ti^{4+},[14-16] such as TaON, Ta_3N_5 and $LaTiO_2N$, emerge as promising candidates for PEC overall water splitting.[17-19] TaON, as a n-type semiconductor, is one promising material that meets many of the requirements for the water

splitting even without external bias using a large portion of the solar spectrum (< 500 nm): (i) it has a suitable band gap of 2.5 eV; (ii) it is feasible to conduct for water splitting due to an appropriate band positions; and (iii) it is composed of nontoxic elements, making it environmentally benign.[20-23] Despite such promising attributes, the overall water splitting efficiency of TaON photoanodes falls well short of the theoretical maximum efficiency, which is possibly limited by several main drawbacks: (i) the low carrier mobility; and (ii) its poor stability due to self-photocorrosion in electrolyte solution.[20-23]

Generally, photocatalyst features such as high crystallinity, low defect density, short charge–transfer distance, large surface area, and special morphology usually enhance the photocatalytic performance. Nanostructured photoelectrodes have begun to address current materials limitations. One–dimensional (1D) nanostructured arrays have the apparent advantages of promoting the transport and separation of photoexcited charge carriers, and providing abundant surface reaction sites, which are crucial for obtaining high solar energy conversion efficiency.[24-27] For examples, polycrystalline Ta_3N_5 nanotube arrays on the Ta substrate were prepared by anodization of tantalum foil.[28-30] Ta_3N_5 nanorod arrays were produced via a through−mask anodization method and a subsequent nitridation process using anodic alumina as the mask under the anodizing voltage of 650 V and a vapor–phase hydrothermal process and subsequent nitridation.[31,38] Besides Ta_3N_5 photoanodes, although 1D TaON nanotube arrays can be prepared,[32] it is still a challenging for the synthesis of a desired 1D TaON nanostructured array using low-cost and easily-scalable routes.

For efficient water splitting using photoanodes, one prospective solution is known as a p–n photochemical diode, promoting the separation of photogenerated electrons and holes, because a single material is unlikely to possess both the narrow bandgap and proper band positions required.

The junction is the one of the design concept to separate electrons and holes by the internal electric field induced from band bending. For examples, the heterojunction films, such as various $WO_3/BiVO_4$,[33] $CaFe_2O_4/ZnFe_2O_4$,[34] $Fe_2O_3/ZnFe_2O_4$,[35] and $CaFe_2O_4$/TaON,[36] have shown promising photoelectrochemical activity, with the improvement ascribed to efficient carrier separation in the heterojunction. In particular, cuprous oxide, Cu_2O, is an attractive p-type oxide for photoelectrochemical hydrogen production with a direct bandgap of 2.0 eV and a corresponding theoretical photocurrent of 14.7 mA cm^{-2} and a light–to–hydrogen conversion efficiency of 18% based on the AM1.5 spectrum since Cu_2O possesses favourable energy band positions, with the conduction band lying 0.7 V negative of the hydrogen evolution potential and the valence band lying just positive of the oxygen evolution potential.[37] Since TaON has conduction and valence band edges at *ca.* −0.3 and +2.2 eV vs. NHE, respectively,[14,20-23] the band gap of TaON is well-matched with Cu_2O for efficient charge carrier separation. Therefore, developing Cu_2O/TaON arrays as a p–n heterojunction photoanode for PEC water splitting is highly desirable.

The practical application of (oxy)nitrides photoelectrodes is hindered by the poor photostability as the serious obstacle. To solve this problem, most efforts about Ta_3N_5 photoanodes have been made on alleviating accumulation of photogenerated holes by facilitating water oxidation using various oxygen evolution reaction (OEC) cocatalysts.[38-42] However, it is also essential to provide a highly stable TaON-based photoelectrodes coupled with the protective layer.[18,19] Besides the OEC catalysts, carbon as a fascinating material has offered exciting new opportunities in various fields of nanotechnology including photocatalysis based on properties such as high electrical conductivity, nontoxicity, high strength, and high chemical stability.[43,44] Especially, it is easy to conduct the carbon layer coating on the nonstable semiconductor-based photoelectrode in a solution-based carbon precursor.[43-46] For examples, Zhu *et al.* reported surface hybridization of TiO_2 with

graphite-like carbon layers of a few molecular layers thickness yields efficient photocatalysts.[43] Alper *et al.* showed an ultrathin graphitic carbon layer on porous silicon nanowires with the high specific capacitance for planar microsupercapacitor electrode.[45] Thus, to the best of our knowledge, no previous work regarding the application of the ultrathin carbon sheath passivated Cu_2O/TaON photoelectrodes with perfect photostability on the efficient photoelectrochemical water oxidation has been reported.

The requirement for nanostructured TaON presents a potential challenge for coupling many well-known water splitting catalysts to the surface. In this work, we report on the fabrication of aligned TaON nanorod arrays using a general vapor–phase hydrothermal route with subsequent nitridation. After the involvement of a $Cu(OH)_2$/TaON nanorod array prepared by a chemical bath deposition process into a carbon precursor based solution, the Cu_2O nanoparticles/TaON nanorod array passivated with ultrathin carbon sheath as a surface protection layer against photocorrosion (carbon–Cu_2O/TaON) was successfully achieved via a subsequent heat-treatment strategy. Especially, the carbon–Cu_2O/TaON nanorod arrays with a metal/co-catalyst-free protective carbon layer as the integrated photoanode by the highly cost-effective and easily scalable approach, are used for solar water splitting to achieve superior enhancement in the photoelectrochemical (PEC) performance with the best durability against photocorrosion to date, which is one of the highest among all the photoanodes so far reported in the field of energy conversion.

2. Experimental Section

2.1 METHODS.

2.1.1 Fabrication of TaON nanorod arrays

Ta foil with a thickness of 0.25 mm (Alfa Aesar) was washed in ethanol, acetone, isopropanol

and deionized water each for 60 minutes before used. The clean Ta foil was suspended above a 0.15 M HF aqueous solution in a Teflon-lined autoclave, which was then heated at 180~240 ^{o}C for 0~6 h to grow F–containing Ta_2O_5 (F–Ta_2O_5) nanorod arrays on the Ta foil.[40] After heat-treatment, the resultant F–Ta_2O_5 nanorod arrays on the Ta foil under a gaseous atmosphere of NH_3 with a flow of 20 mL min^{-1} and heated at 650~750 °C for 3 h, transformed into the formation of TaON nanorod arrays.

2.1.2 Fabrication of carbon–Cu_2O/TaON nanorod arrays

In this typical process, a chemical bath deposition process was developed to decorate Cu_2O nanocrystals onto the surfaces of the TaON nanorod arrays. Typically, as-prepared TaON nanorod arrays were added into an ethanolic solution of 0.04 M $Cu(CH_3COO)_2$, allowing the adsorption and deposition of Cu^{2+} ions onto the surfaces of the TaON nanorod arrays for different times (10, 20, 40 and 60 s). After the Cu^{2+} ion adsorption, the TaON nanorod array was put into a NaOH solution, maintaining at 60 ^{o}C in a water bath for the formation of the $Cu(OH)_2$/TaON nanorod array. Then, an aqueous solution of glucose (5 mL) as carbon precursor with the various concentration (0.01, 0.05, 0.1 and 0.2 M) was slowly added into the above suspension. After ultrasonication for a certain time, the samples were rinsed with distilled water to remove CH_3COO^-, glucose, and NaOH, and then was dried under vacuum at a temperature of 60 ^{o}C for 2 h. Finally, the $Cu(OH)_2$/TaON nanorod arrays with or without glucose were immediately transferred into the furnace and annealed at 500 ^{o}C in N_2 atmosphere for two hours, leading to the achievement of the carbon–Cu_2O/TaON and Cu_2O/TaON nanorod arrays.

2.2 Characterization

The obtained products were characterized with powder X–ray diffraction (XRD, MAC Science Co. Ltd Japan) using Cu K_α (λ = 0.1546 nm) for XRD patterns. The morphology and size of the

resultant powders were characterized by a Zeiss Ultra 55 field–emission scanning electron microscope (SEM) associated with X–ray energy–dispersive spectrometer (EDX). Transmission electron microscopy (TEM) images were captured on the transmission electron microscopy (TEM, JEM–2010) at an acceleration voltage of 200 kV. The chemical states of the sample were determined by X–ray photoelectron spectroscopy (XPS) in a VG Multilab 2009 system (UK) with a monochromatic Al K_α source and charge neutralizer. The optical properties of the samples were analyzed by UV–vis diffuse reflectance spectroscopy using a UV–vis spectrophotometer (UV-2550, Shimadzu). Raman spectroscopy was conducted with a Renishaw LabRAM confocal Raman microscope utilizing a 633 nm laser.

2.3 Photoelectrochemical Water Splitting

The photoelectrochemical water splitting was carried out in a three-electrode system, where the TaON, Cu_2O/TaON and carbon–Cu_2O/TaON photoanodes (the irradiation area was 1 cm^2), a saturated calomel electrode (SCE) and a high surface area platinum mesh act as working electrode, reference electrode and counter electrode, respectively. An aqueous solution of 0.5 M NaOH was used as the electrolyte (pH = 13.6, 100 mL). The electrolyte was stirred and purged with Ar gas before the measurements. The photoanodes were illuminated with AM 1.5G simulated sunlight (100 mW cm^{-2}) from a commercial solar simulator. The measured potential versus SCE was converted to the RHE scale according to the Nernst equation ($E_{RHE} = E_{SCE} + 0.059pH + 0.242$), where E_{RHE} was the potential vs. a reversible hydrogen potential, E_{SCE} was the potential vs. SCE electrode, and pH was the pH value of electrolyte. The wavelength dependent the incident photon to current efficiency (IPCE) was calculated according to the following equation:

$$IPCE(\%) = \frac{1240 \times i_{ph}}{\lambda \times p_{in}} \times 100$$

where i_{ph} is the photocurrent (mA), λ is the wavelength (nm) of incident radiation, and p_{in} is the

incident light irradiance on the semiconductor electrode at the selected wavelength (mW).[47] Photocurrent-potential curves were measured at a rate of 30 mV/s. The wavelength dependence of the incident photon to current efficiency (IPCE) was measured under monochromatic irradiation from a Xe lamp equipped with band-pass filters (central wavelengths: 400, 420, 440, 460, 480, 500, 540, 580 and 600 nm; FWHM: 10 nm).

The hydrogen and oxygen evolution by photoelectrochemical water splitting was conducted in the air-tight reactor connected to a closed gas circulation system. The TaON, Cu_2O/TaON and carbon–Cu_2O/TaON photoanodes were biased at 1.0 V vs. RHE in a stirred aqueous solution of 0.5 M NaOH (pH = 13.6) under AM 1.5G simulated sunlight. The amount of hydrogen or oxygen was determined by a gas chromatography (GC–3240, TCD, Ar carrier). For Faradaic efficiency, a two-electrode cell (no reference electrode) was used to measure the Faradaic efficiency. A carbon–Cu_2O/TaON photoanode and a Pt foil were used as a working electrode and a counter electrode, respectively. The bias was 1.0 V. The area of the carbon–Cu_2O/TaON was about 1 cm^2. The cell was sealed and was purged by Ar for half an hour and no O_2 or N_2 was detected before the Faradaic efficiency measurement.

3. Results and Discussion.

The synthesis process of the Cu_2O nanoparticles/TaON nanorod array passivated with ultrathin carbon sheath as a surface protection layer as an integrated photoanode was presented in scheme 1. Ta foil was selected as the base material for the photoanode based on the following considerations of a conductive substrate and a direct precursor of F–Ta_2O_5 nanorod array grown on the Ta substrate via a vapour–phase hydrothermal induced self-assembly technique (Figure S1-S2). Then the TaON nanorod array with the unique open area was obtained by the subsequent nitridation process.

Employed a chemical bath deposition process, the $Cu(OH)_2$ species were formed on the surface of TaON nanorod array under the involvement of Cu^{2+} ions into NaOH solution. In view of the desirable 1D nanorod structure, it is imperative to maintain the Cu_2O/TaON nanorod array after the deposition of Cu_2O nanoparticles. Finally, the delicate conversion of the $Cu(OH)_2$ to Cu_2O nanoparticles on the surface of TaON nanorod array along with the simultaneous formation of a thin carbon sheatth as a protective layer, as shown in Scheme 1, was achieved by a solution-based carbon precursor coating of the initial $Cu(OH)_2$/TaON nanorod array and subsequent annealing strategy of the glucose–$Cu(OH)_2$/TaON nanorod array under inert N_2 environment, resulting into the formation of the carbon–Cu_2O/TaON nanorod array as integrated photoanode.

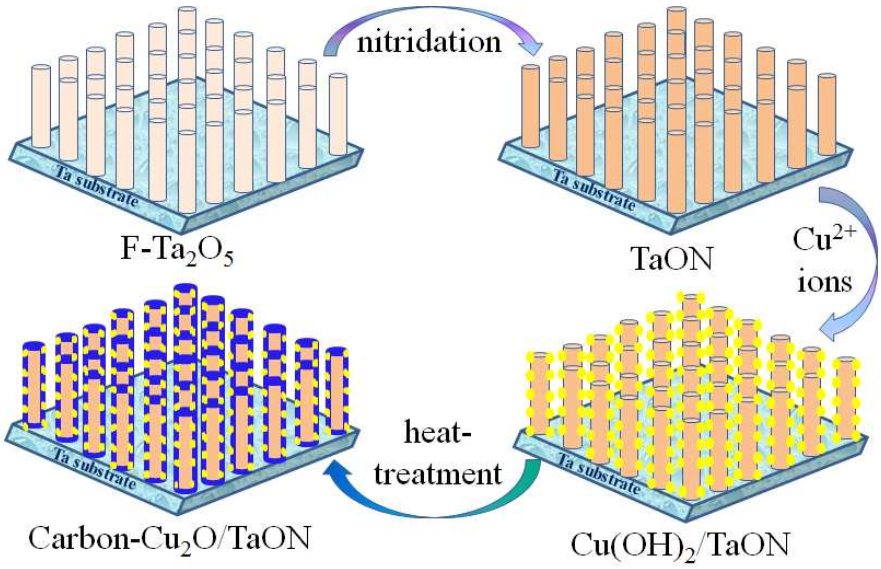

Scheme 1. Schematic illustration of ultrathin carbon sheath passivated Cu_2O/TaON nanorods array.

The top surface view of TaON, Cu_2O/TaON, and carbon–Cu_2O/TaON nanorods array were conducted by field emission scanning electron microscopy (FESEM). From Figure 1a, the TaON nanorods array are vertically aligned on the entire surface of the Ta substrate with uniform nanorods that have an average diameter of 40~60 nm, indicating that the surface of the individual TaON nanorods array is smooth, which is similar with the previous works.[39,40] After the chemical

bath deposition process and the subsequent heat-treatment of the $Cu(OH)_2$/TaON nanorod array, the Cu_2O nanoparticles with an ultra-small particle size were homogeneously formed on the surface of TaON nanorod array, as shown in Figure 1b. During the phase–transformation process, the conversion of $Cu(OH)_2$ to Cu_2O is presumably achieved by dehydration of $Cu(OH)_2$ to CuO, followed by removal of oxygen from the lattice of CuO to form Cu_2O at high temperature in inert N_2 atmosphere.[44] Furthermore, the $Cu(OH)_2$/TaON nanorod array was involved into the glucose solution as carbon precursor, the carbon sheath covered Cu_2O/TaON nanorods array was achieved via the subsequent heat-treatment strategy, as shown in Figure 1c. At the initial stage of the heat-treatment process, the glucose dehydrates and cross-links, and as the reaction continues, aromatization and carbonization take place, resulting in a firm carbonized shell covering the nanorod surfaces, guaranteeing the integrity of the original morphology of the starting $Cu(OH)_2$ species.[44,48] Especially, close observation of the composites of carbon–Cu_2O/TaON nanorod arrays, the Cu_2O nanoparticles are still clearly visible after the carbon coating, indicating that the carbon layer is ultrathin. In order to understand the structure of this heterojunction, the illustration scheme of carbon–Cu_2O/TaON nanorods array was presented in Figure 1d. To confirm the entire quality of carbon–Cu_2O/TaON nanorods array, the surface view with the large magnification of SEM image was also presented in the Figure S3, indicating the whole carbon–Cu_2O/TaON nanorods array maintained the homogeneous 1D morphology after the modification of the Cu_2O nanoparticles and the ultrathin carbon layer. Thus, the rationally designed and synthesized carbon–Cu_2O/TaON nanorods array is expected to work as an efficient and stable photoanode for water splitting application.

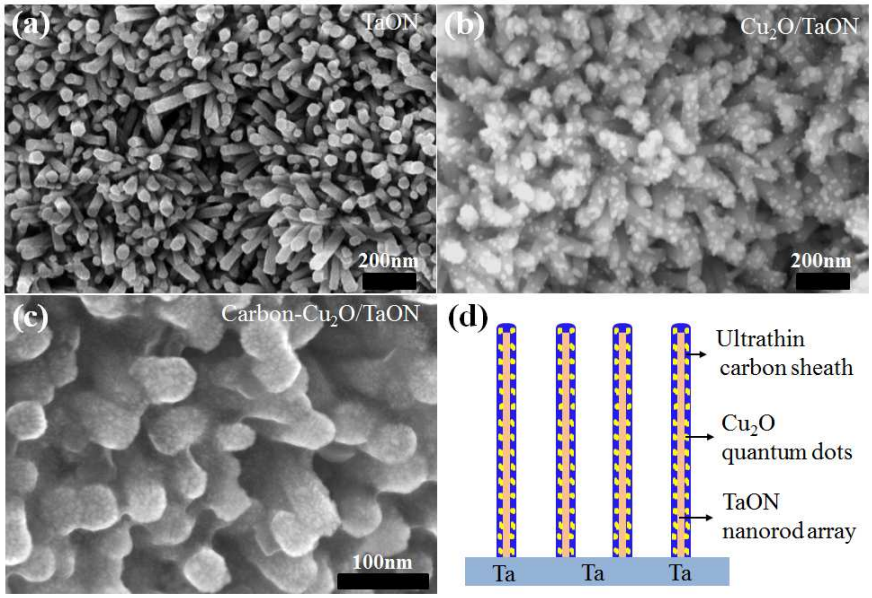

Figure 1. Top surface view of (a) TaON, (b) Cu_2O/TaON, (c) carbon–Cu_2O/TaON nanorods array and (d) illustration scheme of carbon–Cu_2O/TaON nanorods array.

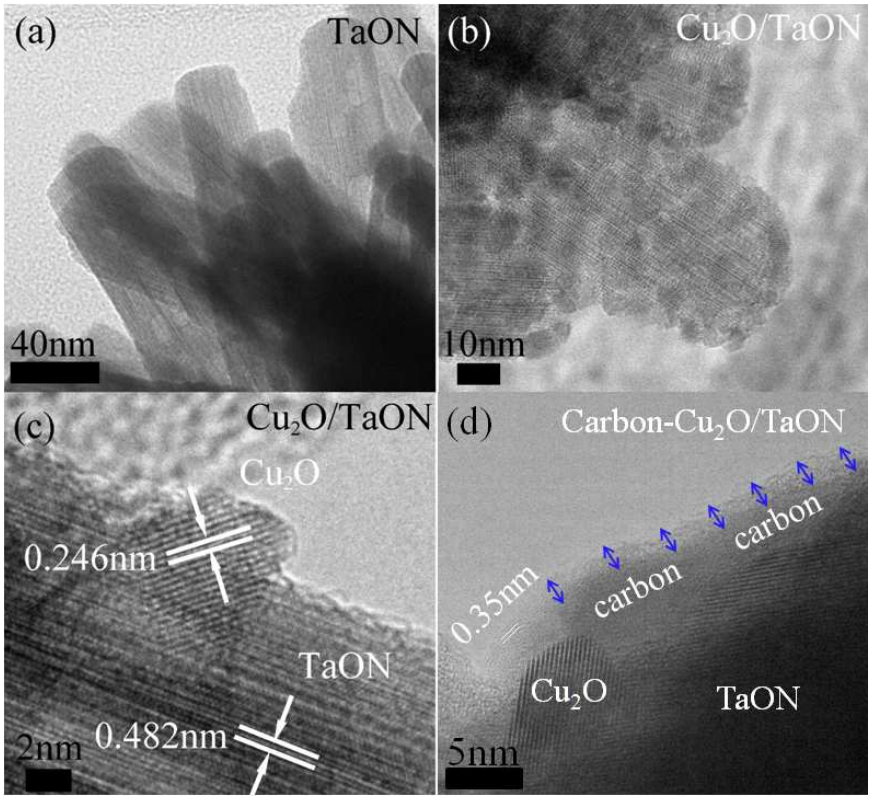

Figure 2. TEM and HRTEM images of different samples. (a) TaON, (bc) Cu_2O/TaON, and (d) carbon–Cu_2O/TaON.

The obtained TaON, Cu_2O/TaON and carbon–Cu_2O/TaON nanorod arrays were further characterized using transmission electron microscopy (TEM) and high–resolution transmission electron microscopy (HRTEM) as well as. TEM image confirms the single–crystal nature of the TaON nanorods and their preferential growth of the [001] direction (Figure 2). After the decoration of Cu_2O, the TEM images of the Cu_2O/TaON heterojunction indicate that the Cu_2O nanoparticles with the average particle size from 3 to 10 nm were homogeneously dispersed on the surface of TaON nanorods, providing the formation of an intact interface between Cu_2O and TaON, where the lattice fringes of 0.246 nm and 0.482 nm corresponded to the refections from the (111) plane of Cu_2O (JCPDS 05−667) and the refections from the (100) plane of TaON (JCPDS 70−1193) from HRTEM image of Cu_2O/TaON (Figure 2bc). Figure 2d shows high– resolution (HR) TEM image of carbon–Cu_2O/TaON which was used to estimate carbon shell thickness, demonstrating that the Cu_2O/TaON nanorod array is surrounded by a few graphitic carbon layers, and the overall thickness of the carbon shell is about ~3 nm. The *d*–spacing of the graphitic layers is 0.35 nm, which is in agreement with the literature. The scanning transmission electron microscope (STEM)–energy dispersive X–ray spectroscopy (EDX) elemental mapping (Figure 3) shows a single carbon–Cu_2O/TaON nanorod with an average diameter of 40~60 nm. In contrast, Figure 3 shows that the carbon sheath and Cu_2O nanoparticles in the carbon–Cu_2O/TaON configuration was very uniform, with the brighter spots in the Ta, Cu, C, O and N elemental mapping showing the distribution of Cu_2O and carbon species. Thus, since the surface of the the Cu_2O/TaON nanorod array is fully covered with a thin graphite-like carbon film, a good electronic contact between (oxy)nitride semiconductor and carbon was achieved.

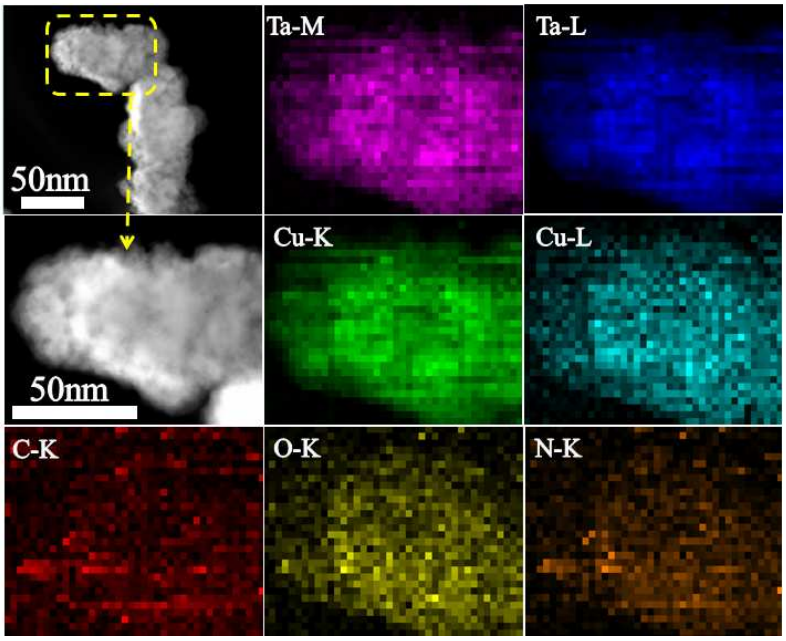

Figure 3. STEM images and corresponding EDX elemental mapping of Ta, Cu, C, O and N of a single carbon–Cu_2O/TaON nanorod.

The phase purity, crystal structure, chemical states of each element and optical properties of the obtained samples were examined by X–ray diffraction (XRD), X–ray photoelectron spectroscopy (XPS) and UV–vis diffuse reflectance spectroscopy (UV–vis DRS). After the chemical bath deposition process, the $Cu(OH)_2$/TaON nanorod array was obtained. According to XRD patterns in Figure 4S, five main diffraction peaks near at 2θ = 23.8, 34.1, 35.9, 39.8 and 53.2^o can be observed, corresponding to (021), (002), (111), (130) and (132) plane diffraction of $Cu(OH)_2$ [JCPDS No.12−420, orthorhombic, space group: $Cmc2_1$], respectively, indicating that the $Cu(OH)_2$ phase was confirmed on the surface of the TaON nanorod array (Figure S4). After the subsequent heat-treatment of the $Cu(OH)_2$/TaON nanorod array, three main diffraction peaks near or at 2θ = 36.4, 42.5 and 61.3^o can be observed, corresponding to (111), (200) and (220) plane diffraction of Cu_2O [JCPDS No. 05−667, cubic, space group: $Pn\bar{3}m$], respectively, confirming the achievement of the transformation of the $Cu(OH)_2$ to Cu_2O phase on the surface of the TaON nanorod (Figure

S4). Moreover, compared to XRD patterns of Cu_2O/TaON, there is no obvious changes in the intensities and widths for carbon–Cu_2O/TaON due to the low loading content of carbon. Especially, the characteristic diffraction peaks of TaON/Ta phase (JCPDS No. 70−1193) are observed and there are no obvious changes of intensities and widths in all samples. In addition, the two strong peaks of (211) and (321) can be indexed to the phase of Ta for all samples. This implies that there is no significant change observed in phase structure and crystallite size of TaON after the co-modification of Cu_2O and carbon. Especially, the XRD patterns of the carbon–Cu_2O/TaON sample indicate that the deposited Cu_2O and carbon species are attached on the surface of TaON nanorod array, which is in agreement with the SEM and TEM measurements.

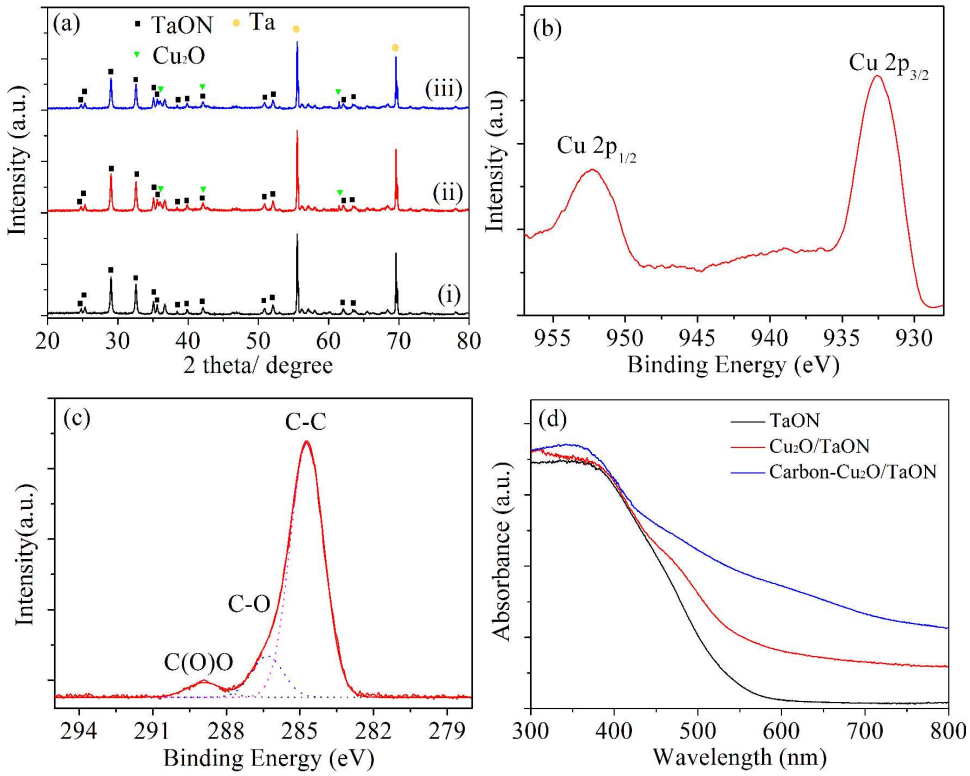

Figure 4. (a) XRD patterns of (i) TaON, (ii) Cu_2O/TaON and (iii) carbon–Cu_2O/TaON photoanodes, (bc) XPS spectra of carbon–Cu_2O/TaON photoanode and (d) UV−vis diffuse reflectance spectra of TaON, Cu_2O/TaON and carbon–Cu_2O/TaON photoanodes.

In order to determine the surface composition and chemical nature of carbon–Cu_2O/TaON composites, the chemical state of each element in the samples were carefully checked by X–ray photoelectron spectroscopy (XPS). XPS characterization was performed, from which survey spectrum, Ta, O, N, C and Cu elements were observed (Figure 4 and Figure S5-6). The binding energies were calibrated by using the contaminating carbon C1s peak at 284.5 eV as a standard. In Figure S5, XPS signals of Ta 4f in the carbon–Cu_2O/TaON composites are observed at binding energies at around 26.0 eV (Ta $4f_{7/2}$) and 27.6 eV (Ta $4f_{5/2}$) ascribed to Ta^{5+}.[20-23] Figure 4b displays the Cu 2p level spectrum. The Cu $2p_{3/2}$ and Cu $2p_{1/2}$ spin–orbital photoelectrons were located at binding energies of 932.5 eV and 952.4 eV, respectively, which are in good agreement with the reported values of Cu_2O.[44] Obviously, the deposited nanoparticles were Cu_2O rather than Cu or CuO. Especially, after the combination of the ultrathin carbon on the surface of Cu_2O/TaON, the strong C−C peak at 285.0 eV implies the formation of a carbon layer on the surface of Cu_2O/TaON, as shown in Figure 4c. Furthermore, a notable decrease in oxygen content is clearly visible and the peak corresponding to the C−O bond has disappeared in Figure 4c, compared with the extensive results of carbon.[49] The oxygen loss mainly results from the loss of C−O and O−C=O, indicating the partial removal of the oxygen-containing functional groups, which is in agreement with the literature.[49]

For the optical properties of the samples, it is observed that the absorption onset of the pure TaON nanorod array was at approximately 500~550 nm, which agreed well with the bandgap of bulk TaON (E_g = 2.5 eV).[14] With regard to Cu_2O/TaON, due to the narrow bandgap of Cu_2O (E_g = 2.0 eV),[37] the Cu_2O/TaON nanorod array displayed red shifts in the bandgap transition and an enhanced absorption in the visible-light region, shown in Figure 4d. After the coating of the ultrathin carbon sheath using the solution-based carbon precursor coating (i.e., glucose solution)

combined with subsequent carbonization strategy, the carbon–Cu_2O/TaON presents the enhanced absorption in the long wavelength region due to the strong absorption of the carbon layer. This suggests an increased electric surface charge of the semiconductor within the carbon–Cu_2O/TaON composite due to the introduction of the carbon which can possibly cause modifications of the fundamental process of electron–hole pair formation during irradiation.

PEC measurements was carried out in a three–electrode system for the TaON nanorod arrays as the working electrode with an exposed area of 1 cm^2, a Pt foil as the counter electrode, a saturated calomel electrode (SCE) as a reference electrode, and the NaOH electrolyte (0.5 M, pH = 13.6). The photocurrent density versus applied voltage scans of the samples were measured under AM 1.5G simulated sunlight (100 mW cm^{-2}). As shown in Figure 5a, the bare TaON photoanode presented at the negligible current in the dark. However, the bare TaON nanorod array photoanode reached 0.63 mA cm^{-2} at 1.0 V vs. RHE and even 0.93 mA cm^{-2} at 1.23 V vs. RHE under AM 1.5G simulated sunlight (100 mW cm^{-2}), which is ascribed to the serious recombination and photocorrosion during the slow interface charge transfer process since the photogenerated holes are accumulated on the surface of the TaON photoanode. After the modification of Cu_2O nanoparticles, the Cu_2O/TaON nanorod array yielded the photocurrent density of 2.12 mA cm^{-2} at 1.0 V vs. RHE and even 2.94 mA cm^{-2} at 1.23 V vs. V_{RHE} under AM 1.5G solar light, which are higher than that of $CaFe_2O_4$/TaON photoanode (1.26 mA cm^{-2} at 1.23 V vs. V_{RHE}).[17] Moreover, the Cu_2O/TaON nanorod array passivated with ultrathin carbon sheath (carbon–Cu_2O/TaON) exhibits the photocurrent of 3.06 mA cm^{-2} at 1.0 V vs. RHE and even 4.36 mA cm^{-2} at 1.23 V vs. V_{RHE} under AM 1.5G solar light, which are almost five times higher than that of bare TaON photoanode. Obviously, it is evident that the sharp rise beyond the onset potential and the tendency for photocurrent in the high-potential region indicate high charge transfer and collection efficiency for

carbon–Cu_2O/TaON photoanode. Specially, the photocurrent density of the carbon–Cu_2O/TaON heterostructured photoanode is 1.5~5.4 mA cm^{-2} in the potential range of 0.8~1.5 V vs. RHE under AM 1.5G 100 mW cm^{-2} simulated sunlight, exhibiting that not only the onset potential is negatively shifted but also the photocurrent is significantly improved due to the effective charge transfer process.

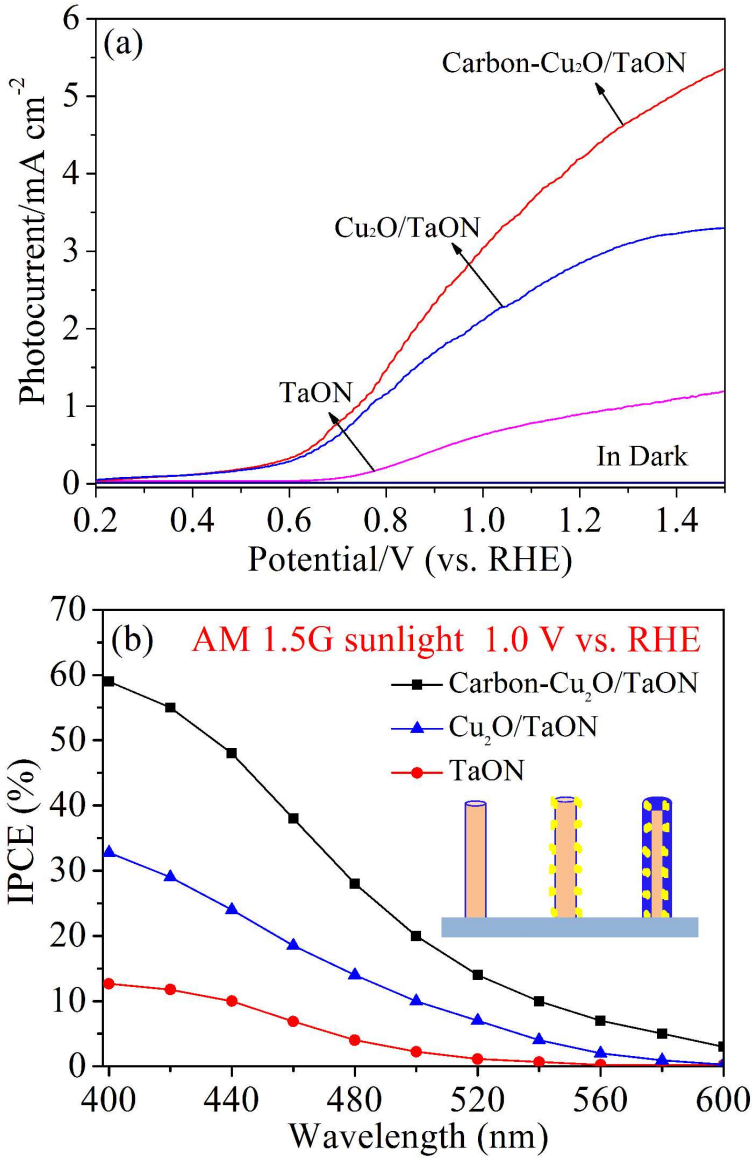

Figure 5. (a) Photocurrent–potential curves in the dark and under AM 1.5G simulated sunlight (100 mW cm^{-2}), and (b) the incident photon to current efficiency (IPCE) at 1.0 V vs. RHE under monochromatic irradiation for TaON, Cu_2O/TaON and carbon–Cu_2O/TaON photoanodes.

To verify the above photocurrents under AM 1.5 G simulated sunlight condition, the incident photon to current efficiency (IPCE) of the TaON, Cu_2O/TaON and carbon–Cu_2O/TaON photoanodes, has been measured under monochromatic light irradiation and plotted as a function of wavelength at given voltage (Figure 5b). At an applied potential of 1.0 V vs. RHE, the IPCEs for the carbon–Cu_2O/TaON photoelectrode were above 48% in the range of 400~440 nm, which is higher than that of CoO_x/TaON electrode (*ca.* 42% at 400 nm at 1.2 V vs RHE in sodium phosphate buffer solution) and that of $CaFe_2O_4$/TaON electrode (*ca.* 30% at 400 nm at 1.23 V vs RHE in 0.5 M NaOH solution) in the previous work.[17,18] However, it is lower than that of IrO_x/TaON electrode (*ca.* 76% at 400 nm at 1.15 V vs RHE in Na_2SO_4 solution), while the photocurrent of the IrO_x/TaON photoanode was decreased remarkably due to the self-oxidative deactivation of the TaON surface.[19] In addition, among the wavelength range of 500~600 nm, the IPCEs for the carbon–Cu_2O/TaON photoelectrode were 3~20% while below 2.2% for the TaON photoanode, indicating the carbon–Cu_2O/TaON photoanode presented the enhanced IPCEs in the long wavelength region due to the red shifts in the bandgap transition from the introduction of Cu_2O nanoparticles and the strong absorption of the carbon sheath, which is in agreement with the distribution of the UV–vis diffuse reflectance spectra. It is worth to pointing out that a maximum IPCE of 59% was achieved at 400 nm for the carbon–Cu_2O/TaON photoanode. Thus, the combined results demonstrate that the recombination of photoexcited carriers is effectively inhibited through the modification of Cu_2O nanoparticles and ultrathin carbon layer which can accelerate the water splitting reaction and improve the charge transfer processes.

It is well-known that the practical application of (oxy)nitrides photoelectrodes during water splitting reaction is hindered due to the poor photocurrent stability as the serious obstacle.[13-19] After the enhancement of photocurrent through the TaON nanorod array, the major aim of this work is to

improve the photostability of the TaON nanorod array photoanode. Compared with the photocurrent densities of bare TaON, Cu_2O/TaON and carbon–Cu_2O/TaON photoelectrodes in NaOH (pH = 13.6) solution at 1.0 V vs. RHE under AM1.5G illumination (100 mW cm^{-2}) for 60 min, the effect of Cu_2O nanoparticles and ultrathin carbon layer on the photostability of TaON nanorod array was examined. As shown in Figure 6a, the photocurrent generated by the bare TaON array decreases significantly within a short times, and the steady state photocurrent is negligibly low in few seconds, indicating that accumulation of photogenerated holes at the surface of TaON due to poor kinetics for water splitting and subsequent surface oxidative decomposition of TaON.[20-23] After the modification of Cu_2O nanoparticles, the Cu_2O/TaON photoanode exhibits almost 46.7% of the initial stable photocurrent of ~2.12 mA cm^{-2} under AM1.5G irradiation for 60 min at 1.0 V vs. RHE, resulting into the improvement of photostability in NaOH solution. To examine the reason behind it, the Auger Cu LMM spectra (Figure S7) were used to show the surface change after the stability test. No peak related to Cu(0) emerged in the Cu LMM spectra of Cu_2O/TaON and carbon-Cu_2O/TaON after the stability test. Combined with the previous works about poor stability of Cu_2O,[37,44] the limited enhancement of photostability for the Cu_2O/TaON photoanode is ascribed to the phase conversion because the accumlated surface holes lead to the oxidation of Cu_2O and a certain of photocorrosion of TaON because Cu_2O nanoparticles doesn't fully cover TaON nanorods. Noticeably, almost 87.3% of the initial stable photocurrent of ~3.06 mA cm^{-2} for carbon-Cu_2O/TaON photoanodes, remains under AM1.5G irradiation for 60 min at 1.0 V vs. RHE, indicating that the ultrathin carbon layer efficiently restrain the recombination pathways and improve the kinetic transport of photogenerated charge carriers for the carbon–Cu_2O/TaON photoanode. Furthermore, the Cu 2p XPS spectra of carbon-Cu_2O/TaON photoanode was also shown in Figure S8b after the Faradaic efficiency test. The peaks at 932.4 and 952.2 eV correspond

to the binding energy of Cu $2p_{3/2}$ and Cu $2p_{1/2}$ of Cu_2O, and those at 934.3 and 953.8 eV are attributed to CuO,[51,52] confirming the coexistence of a trace amount of CuO. Thus, there is still a certain decrease of the photocurrent in the carbon–Cu_2O/TaON photoanode, which may be ascribed to the little oxidation of Cu_2O and the charge recombination or other mechanisms, such as photon exchange, tunneling through the electric potential barrier near the interface, or thermionic emission.[50] The in-depth research about these mechanisms is beyond the scope of our present work, but efforts will be conducted in the future. Therefore, compared with that of $CaFe_2O_4$/TaON, CoO_x/TaON and IrO_x/TaON photoanode,[17-19] this modified approach using the Cu_2O nanoparticles and ultrathin carbon layer has presented the significant enhancement of the photocurrent and stability of the TaON based photoanodes due to a high built-in potential in the protective p–n heterojunction device encapsulated in an ultrathin graphitic carbon sheath from the electrolyte.

To further explore the effect of the content of Cu_2O nanoparticles and carbon upon the photocurrent densities and photostability of the Cu_2O/TaON and carbon–Cu_2O/TaON photoanodes as a function of the deposition time of Cu^{2+} and the glucose concentration were also investigated in this work, as shown in Figure S9 and S10. The Cu_2O/TaON and carbon–Cu_2O/TaON photoanodes using the 40 s deposition time of Cu^{2+}, and the 0.1 M glucose concentration, exhibited the superior PEC performance. Especially, the carbon–Cu_2O/TaON photoanode demonstrated the highest photocurrent densities of 4.36 mA cm^{-2} at 1.23 V vs. V_{RHE} and the best photostability of 87.3% at 1.0 V vs. V_{RHE} under AM 1.5G solar light, which are ~4.69 times in the photocurrent density and ~14.55 times in the photostability higher than that of bare TaON photoanode. However, the other photoelectrode with the various concentration of glucose and the deposition time, presented the relative decrease of the photocurrent densities and photostability. The above-mentioned results indicate that the combination of the Cu_2O nanoparticles and the carbon sheath with the appropriate

content are indeed an effective strategy for improving the photocurrent density and combating the photocorrosion problem of this TaON photoanode. Thus, the rationally designed and synthesized carbon–Cu_2O/TaON nanorod array is expected to work as an efficient and stable photoanode for water splitting application because (i) the TaON nanorod array with a high surface area provide more contact with electrolyte; (ii) the 1D p-Cu_2O/n-TaON heterostructures facilitates carrier diffusion; (iii) the ultrathin carbon sheath serves as a protective film, preventing the electrolyte from contacting semiconductors; and (iv) the carbon sheath facilitates charge transfer into the electrolyte solution during photoelectrochemical water splitting.

To verify that the measured photocurrent of the carbon–Cu_2O/TaON photoanode originates from water splitting rather than any other undesired side reactions, the oxygen evolution reaction and hydrogen evolution reaction are examined (Figure 6b). The carbon–Cu_2O/TaON photoanode was held at 1.0 V versus RHE under AM 1.5G for 60 min. The amounts of H_2 and O_2 evolved from the carbon–Cu_2O/TaON heterostructured photoanode were 46.5 and 23.1 μmol cm^{-2}, respectively. The ratio of evolution rates of H_2 and O_2 is almost close to the stoichiometric value of 2.0. Faradaic efficiencies of 93% and 90%, respectively, are obtained as determined by measurement of the evolved H_2 and O_2 gas, indicating that the photocurrent is indeed due to the oxygen evolution reaction (OER) and hydrogen evolution reaction (HER). Thus, the above–mentioned results of the Cu_2O nanoparticles and ultrathin carbon layer on TaON nanorod array as integrated photoanode, indicate that the combination of the Cu_2O nanoparticles and ultrathin carbon layer can not only shorten the travel length for charge carriers, but also passivate some surface defects, efficiently suppressing the bulk recombination and surface recombination of the photogenerated charges.

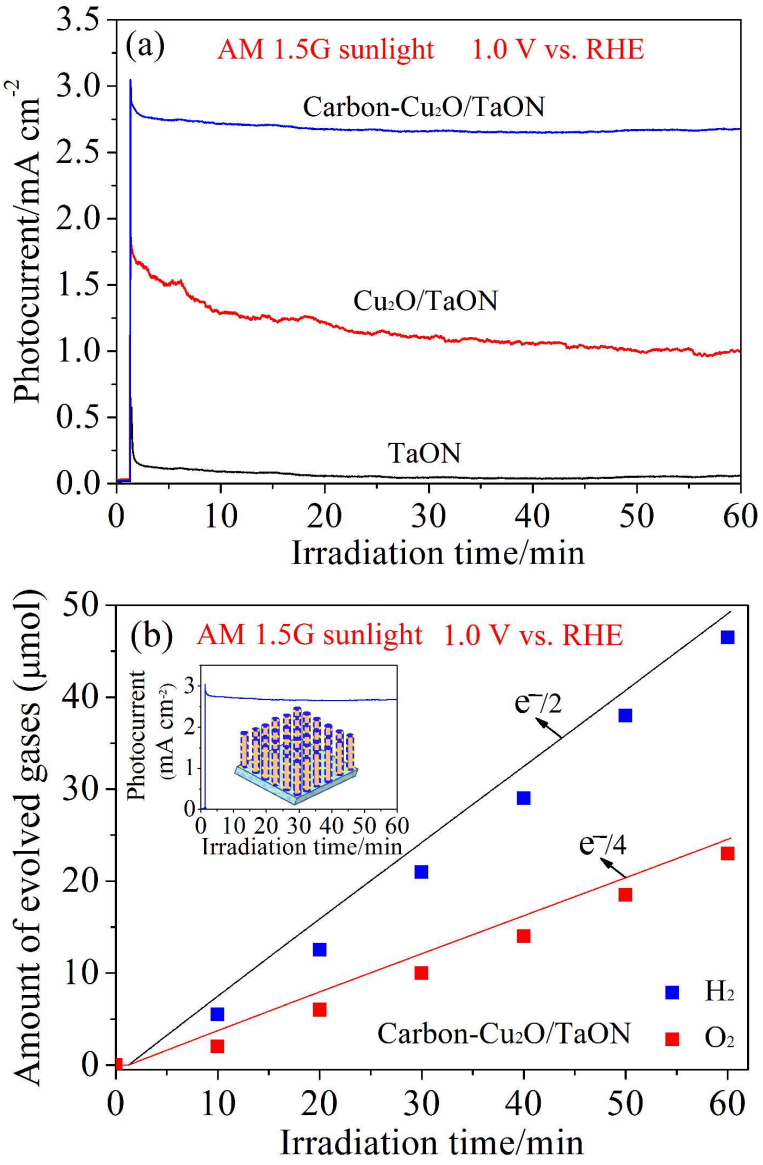

Figure 6. (a) Time courses for the photocurrent of the TaON, Cu_2O/TaON and carbon–Cu_2O/TaON nanorod arrays and (b) gas chromatography of the oxygen and hydrogen evolved from the carbon–Cu_2O/TaON photoanodes at 1.0 V vs. RHE under AM 1.5G simulated sunlight at 100 mW cm^{-2}.

The interfacial properties between the photoelectrodes (i.e., the TaON, Cu_2O/TaON and carbon–Cu_2O/TaON nanorod arrays) and the electrolyte were scrutinized by electrochemical impedance spectroscopy (EIS) measurement that was carried out covering the frequency range of

10^4~0.1 Hz using an amplitude of 10 mV at the open circuit potential of the system. A semicircle (i.e., the arch in the present study) in the Nyquist plots, where x– and y–axes are the real part (Z′) and the negative of imaginary part (−Z″) of impedance, represents the charge–transfer process, while the diameter of the semicircle reflects the charge-transfer resistance (Figure 7). It is well konwn that a large value of impedance indicates a poor conductivity along the electron pathway in the photoelectrode, so it is essential to conduct the fitting of raw data to an equivalent circuit model for the EIS analysis. In this work, the obtained results were fitted into the models of two RC circuits, as shown in Figure 7. The RC circuit with the largest resistance usually represents electrode–electrolyte interface, and the other are related to the electron transport inside the electrode. The first RC circuit presents the electron transport from TaON nanorods arrays to Ta substrate. Clearly, the arches for TaON nanorods arrays under AM 1.5G simulated sunlight were much smaller than those for TaON in the dark because the impedance of TaON-as deposited electrode was too large as compared to the other electrodes to show the all plots in the same scale. When carbon and Cu_2O nanoparticles were introduced into the TaON system, it can be seen that another RC circuit occurs, indicating that the resistance decreased to a large extent. Compared to the TaON, Cu_2O/TaON and carbon–Cu_2O/TaON nanorod arrays under AM 1.5G simulated sunlight, it is obvious that the arches for carbon–Cu_2O/TaON nanorod were much smaller than that of TaON, Cu_2O/TaON nanorod arrays, implying that the decoration with the carbon and Cu_2O nanoparticles significantly reduced the resistance on the movement of charge carriers due to the high electrical conductivity of carbon and the fast transport of charge carriers from the p–n junction formation of Cu_2O/TaON.

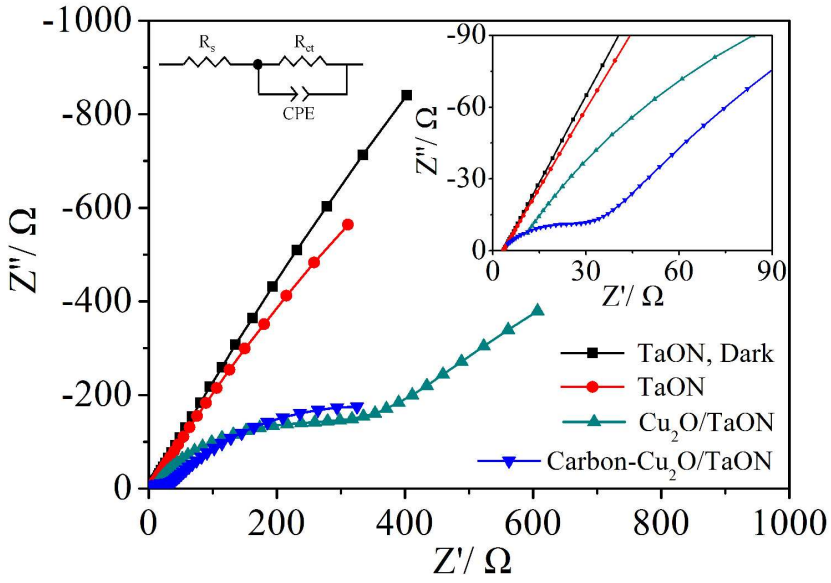

Figure 7. Nyquist plot measured at an applied potential of 1.0 V vs. RHE AM 1.5G simulated sunlight at 100 mW cm^{-2} for the TaON, Cu_2O/TaON and carbon–Cu_2O/TaON nanorod arrays. The inset is the magnified Nyquist plot for the various photoanodes.

Based on the above–mentioned results, a possible PEC water splitting mechanism is proposed in Scheme 2. Although the TaON nanorod array with the relative low IPCE was obtained due to the low transfer of charge carriers and the poor photostability of TaON itself. After the decoration of Cu_2O nanoparticles, the Cu_2O/TaON nanorod array as p–n heterojunction photoelectrode was formed via the chemical bath deposition process and subsequent anealing, corresponding the enhanced photocurrent density, since the Cu_2O/TaON heterojunction structure results into more efficient utilization of incoming light than when only TaON is used for photoanode. Moreover, electrons from Cu_2O move toward Ta substrate through TaON, and holes from TaON migrate to surface of Cu_2O according to the potential difference of Cu_2O (E_g = 2.0 eV, E_{CB} = −0.7 and E_{VB} = +1.3 eV)[37] and TaON (E_g = 2.5 eV, E_{CB} = −0.3 and E_{VB} = +2.2 eV).[14] Thus, the Cu_2O/TaON heterojunction photoanode can not only absorb more visible light, but also improve the efficient charge separation across the junction structure for the PEC water splitting performance. Besides, the

relative medium transfer of charge carriers is ascribed to the improved photostability of TaON and the nice conductive interlayer between the photoelectrode and the substrate. To further improve the photocurrent and photostability of Cu_2O/TaON photoanodes, the ultrathin carbon layer in the carbon–Cu_2O/TaON photoanode behave as an electron conductor to enhance the electron–hole separation and easily transfer the electrons from the conduction band of Cu_2O nanoparticles to the conduction band of the TaON nanorod array and then flow to the Ta substrate along the TaON nanorods, providing a conductive electron transport "highway". The electrons ultimately transfer to the Pt counter electrode to reduce water. At the same time, the O_2 production was produced by the oxidation of water using the accumulated holes on the protective surface of the Cu_2O nanoparticles encapsulated in an ultrathin graphitic carbon sheath. Currently, the nature of the carbon present in the carbon-Cu_2O/TaON samples with two peaks around 1341 and 1596 cm^{-1} was shown by Raman spectra (Figure S11), confirming the presence of sp^2 carbon-type structures within the carbonaceous wall of the carbon-Cu_2O/TaON samples. Thus, it is crucial to effectively separate the photogenerated electron–hole pairs for the enhancement of PEC activity. To a certain extent, the introduction of carbon and the formation of the Cu_2O/TaON heterojunction photoanode facilitate the enhancement in the efficiency of PEC performance. Therefore, the carbon–Cu_2O/TaON photoanode with the unique 1D heterojunction structure feature passivated with ultrathin carbon sheath as a surface protection layer against corrosion, integrating the advantages of enhanced light absorption, rapid charge separation and transport, large contact area and abundant hetero–interfaces, is more favorable to the migration of photogenerated electron–hole pairs, which contribute to the high PEC activity and photostability for water splitting.

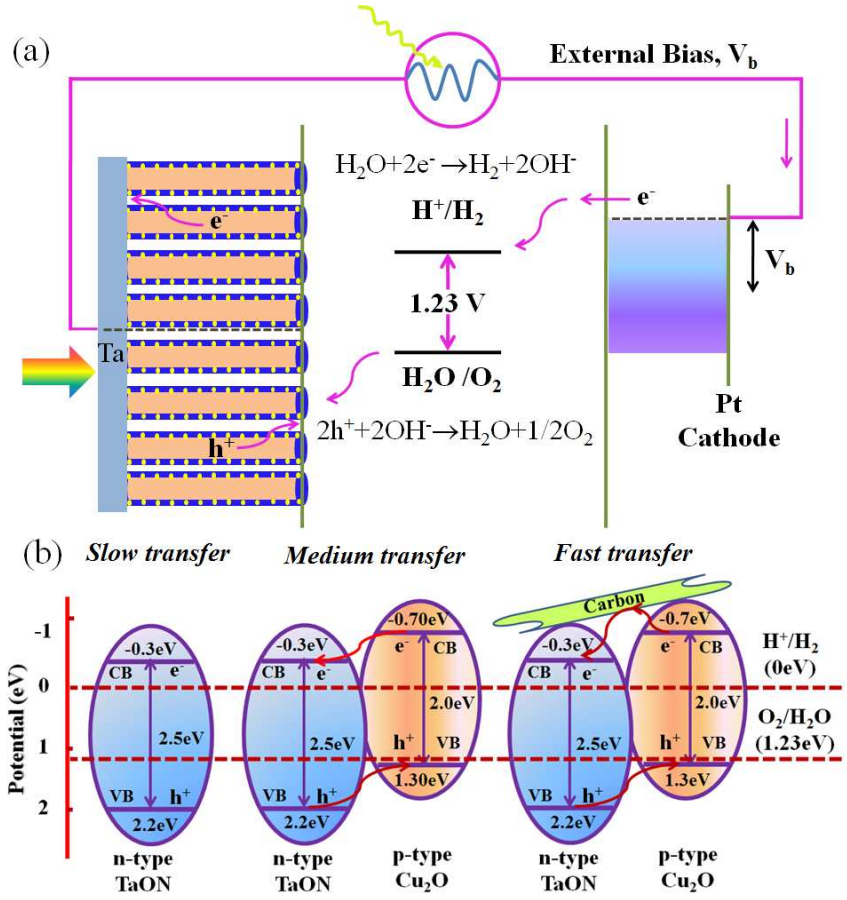

Scheme 2. Schematic for (a) the proposed mechanism of PEC water splitting and (b) the energy band structure of the TaON, Cu_2O/TaON and carbon–Cu_2O/TaON heterojunction photoanodes.

In summary, we have demonstrated a promising strategy for fabricating 1D carbon–Cu_2O/TaON photoanode. The resulting heterojunction exhibited significantly enhanced PEC water oxidation performance, including a large photocurrent density and high stability, which is superior to reported TaON-based photoelectrodes. The enhanced light harvesting, efficient separation of photogenerated electron-hole pairs, fast charge transfer at the interface, and the unique 1D heterojunction nanostructural feature of the 1D Cu_2O/TaON photoanode as the protective p–n heterojunction device encapsulated in an ultrathin graphitic carbon sheath from the electrolyte, contribute to the excellent PEC activity for water oxidation. Our results demonstrated remarkable strategies for

designing and constructing heterojunction photoelectrodes toward practical sunlight-driven PEC water splitting.

Acknowledgements

This work was supported by National Science Foundation of China (No. 51472027 and 51102015), Beijing High School Youth Talent Plan (YETP0351) and National Basic Research Program of China (973 Program, No. 2013CB632404).

Supporting Information Available: XRD pattern, EDS spectra, SEM image, XPS spectra, Raman spectra, Auger Cu LMM spectra, and photocurrent densities. This material is available free of charge via the Internet.

Broader context

With the increasing interest in solar energy utilization for energy crises, the solar water splitting to form hydrogen and oxygen is one of the promising approach that can mimic natural photosynthesis to directly harvest and convert solar energy into clean and sustainable hydrogen energy. Tantalum oxynitride (TaON) semiconductors are potential candidates of photoanode materials because of the narrow bandgap allowing visible light absorption and the appropriate band levels for water splitting. However, the high recombination rate of photoexcited electron–hole pairs and the poor photostability greatly limited their practical applications. In the present work, we have designed and fabricated the p-type Cu_2O /n-type TaON heterojunction nanorod array passivated with ultrathin carbon sheath as a surface protection layer, exhibiting that not only the onset potential is negatively shifted but also the photocurrent and photostability are significantly improved in comparison to that of TaON and Cu_2O/TaON due to a high built-in potential in the protective p–n heterojunction device encapsulated in an ultrathin graphitic carbon sheath from the electrolyte. To help guide continuing research in this field, we identify key challenges that must be overcome to drive down the possible application of oxynitride photoanodes for PEC water splitting.

Reference

1 M. G. Walter, E. L. Warren, J. R. McKone, S. W. Boettcher, Q. Mi, E. A. Santori, N. S. Lewis, *Chem. Rev*., 2010, **110**, 6446−6473.

2 A. J. Nozik, J. Miller, *Chem. Rev*., 2010, **110**, 6443−6445.

3 Z. Li, W. Luo, M. Zhang, J. Feng, Z. Zou, *Energy Environ. Sci*., 2013, **6**, 347−370.

4 K. Sivula, F. Le Formal, M. Gratzel, *Chem. Sus. Chem*., 2011, **4**, 432−449.

5 H. Jun, B. Im, J. Y. Kim, Y. O. Im, J. W. Jang, E. S. Kim, J. Y. Kim, H. J. Kang, S. J. Hong, J. S. Lee, *Energy Environ. Sci*., 2012, **5**, 6375−6382.

6 M. Xu, P. M. Da, H. Y. Wu, D. Y. Zhao, G. F. Zheng, *Nano Lett*., 2012, **12**, 1503−1508.

7 M. D. Ye, J. J. Gong, Y. K. Lai, C. J. Lin, Z. Q. Lin, *J. Am. Chem. Soc*., 2012, **134**, 15720−15723.

8 B. Marsen, E. L. Miller, D. Paluselli, R. E. Rocheleau, *Int. J. Hydrogen Energy*, 2007, **32**, 3110−3115.

9 S. J. Hong, H. Jun, P. H. Borse, J. S. Lee, *Int. J. Hydrogen Energy*, 2009, **34**, 3234−3242.

10 Y. H. Ng, A. Iwase, A. Kudo, R. Amal, *J. Phys. Chem. Lett.*, 2010, **1**, 2607−2612.

11 A. Iwase, A. Kudo, *J. Mater. Chem.*, 2010, **20**, 7536−7542.

12 S. J. Hong, S. Lee, J. S. Jang, J. S. Lee, *Energy Environ. Sci.*, 2011, **4**, 1781−1787.

13 K. Maeda, K. Domen, *J. Phys. Chem. C*, 2007, **111**, 7851−7861.

14 G. Hitoki, T. Takata, J. N. Kondo, M. Hara, H. Kobayashi, K. Domen, *Chem. Commun.*, 2002, 1698−1699.

15 G. Hitoki, A. Ishikawa, T. Takata, J. N. Kondo, M. Hara, K. Domen, *Chem. Lett.*, 2002, **31**, 736−737.

16 A. Kasahara, K. Nukumizu, G. Hitoki, T. Takata, J. N. Kondo, M. Hara, H. Kobayashi, K. Domen, *J. Phys. Chem. A*, 2002, **106**, 6750−6753.

17 E. S. Kim, N. Nishimura, G. Magesh, J. Y. Kim, J. W. Jang, H. Jun, J. Kubota, K. Domen, J. S. Lee, *J. Am. Chem. Soc.*, 2013, **135**, 5375−5383.

18 M. Higashi, K. Domen, R. Abe, *J. Am. Chem. Soc*., 2012, **134**, 6968−6971.

19 R. Abe, M. Higashi, K. Domen, *J. Am. Chem. Soc*., 2010, **132**, 11828−11829.

20 M. Higashi, K. Domen, R. Abe, *Energy Environ. Sci.*, 2011, **4**, 4138−4147.

21 a) J. G. Hou, Z. Wang, S. Q. Jiao, H. M. Zhu, *J. Mater. Chem.*, 2012, **22**, 7291−7299; b) Z. Wang, J. G. Hou, C. Yang, S. Q. Jiao and H. M. Zhu, *Chem. Commun.*, 2014, **50**, 1731−1734; c) J. G. Hou, Z. Wang, R. Cao, S. Q. Jiao and H. M. Zhu, *Dalton Trans.*, 2011, **40**, 4038−4041; d) J. G. Hou, C. Yang, Z. Wang, Q. Ji, Y. Li, G. Huang, S. Q. Jiao, H. M. Zhu, *Appl. Catal. B-Environ.*, 2013, **142**–**143**, 579–589.

22 M. Liao, J. Feng, W. Luo, Z. Wang, J. Zhang, Z. Li, T. Yu, Z. Zou, *Adv. Funct. Mater.*, 2012, **22**, 3066−3074.

23 Hara, M.; Chiba, E.; Ishikawa, A.; Takata, T.; Kondo, J. N.; Domen, K. *J. Phys. Chem. B*, **2003**, *107*, 13441−13445.

24 X. Wang, H. Zhu, Y. Xu, H. Wang, Y. Tao, S. Hark, X. Xiao, Q. Li, *ACS Nano*, **2010**, **4**, 3302−3308.

25 E. S. Smotkin, S. Cervera-March, A. J. Bard, A. Campion, M. A. Fox, T. Mallouk, S. E. Webber, J. M. White, *J. Phys. Chem.*, 1987, **91**, 6−8.

26 Z. Shao, W. Zhu, Z. Li, Q. Yang, G. Wang, *J. Phys. Chem. C*, 2011, **116**, 2438−2442.

27 H. M. Chen, C. K. Chen, C. C. Lin, R. S. Liu, H. Yang, W. S. Chang, K. H. Chen, T. S. Chan, J. F. Lee, D. P. Tsai, *J. Phys. Chem. C*, 2011, **115**, 21971−21980.

28 Y. Cong, H. S. Park, H. X. Dang, F. R. F. Fan, A. J. Bard, C. B. Mullins, *Chem. Mater.*, 2012, **24**, 579−586.

29 X. Feng, T. J. LaTempa, J. I. Basham, G. K. Mor, O. K. Varghese, C. A. Grimes, *Nano Lett.*, 2010, **10**, 948−952.

30 Y. Cong, H. S. Park, S. Wang, H. X. Dang, F. R. F. Fan, C. B. Mullins, A. J. Bard, *J. Phys. Chem. C*, 2012, **116**, 14541−14550.

31 Y. Li, T. Takata, D. Cha, K. Takanabe, T. Minegishi, J. Kubota, K. Domen, *Adv. Mater.*, 2013, **25**, 125−131.

32 S. Banerjee, S. K. Mohapatra, M. Misra, *Chem. Commun.*, 2009, 7137−7139.

33 J. Su, L. Guo, N. Bao, C. A. Grimes, *Nano Lett.*, 2011, **11**, 1928−1933.

34 J. Y. Cao, J. J. Xing, Y. J. Zhang, H. Tong, Y. P. Bi, T. Kako, M. Takeguchi, J. H. Ye, Langmuir, 2013, **29**, 3116−3124.

35 K. J. McDonald, K. S. Choi, *Chem. Mater.*, 2011, **23**, 4863−4869.

36 E. S. Kim, N. Nishimura, G. Magesh, J. Y. Kim, J-W. Jang, H. Jun, J. Kubota, K. Domen, J. S. Lee, *J. Am. Chem. Soc.*, 2013, **135**, 5375−5383.

37 A. Paracchino1, V. Laporte, K. Sivula, M. Grätzel, E. Thimsen, *Nat. Mater.*, 2011, **10**, 456−461.

38 Y. Li, L. Zhang, A. Torres-Pardo, J. M. González-Calbet, Y. Ma, P. Oleynikov, O. Terasak, S. Asahina, M. Shima, D. Cha, L. Zhao, K. Takanabe, J. Kubota, K. Domen, Nat. Comm., 2013, **4**, 2566.

39 C. Zhen, L.Wang, G. Liu, G. Q. Lu, H. M. Cheng, *Chem. Commun.*, 2013, **49**, 3019−3021.

40 J. G. Hou, Z.Wang, C. Yang, H. J. Cheng, S. Q. Jiao, H. M. Zhu, *Energy Environ. Sci.*, 2013, **6**, 3322−3330.

41 M. Li, W. Luo, D. Cao, X. Zhao, Z. Li, T. Yu, Z. Zou, *Angew. Chem. Int. Ed.*, 2013, **52**, 11016−11020.

42 G. J. Liu, J. Y. Shi, F. X. Zhang, Z. Chen, J. F. Han, C. M. Ding, S. S. Chen, Z. L. Wang, H. X.

Han, C. Li, *Angew. Chem. Int. Ed.*, 2014, **53**, 7295−7299.

43 L.W. Zhang, H. B. Fu, Y. F. Zhu, *Adv. Funct. Mater.*, 2008, **18**, 2180–2189.

44 Z. H. Zhang, R. Dua, L. B. Zhang, H. B. Zhu, H. N. Zhang, P. Wang, *ACS Nano*, 2013, **7**, 1709–1717.

45 J. P. Alper, S. Wang, F. Rossi, G. Salviati, N. Yiu, C. Carraro, R. Maboudian, *Nano Lett.*, 2014, **14**, 1843−1847.

46 Y. Wang, H. J. Zhang, L. Lu, L. P. Stubbs, C. C. Wong, J. Lin, *ACS Nano*, 2010, **4**, 4753–4761.

47 M. Sunkara, E. W. McFarland, K. Domen, E. L. Miller, J. A. Turner, H. N. Dinh, *J. Mater. Res.*, 2010, **25**, 3–16.

48 H. J. Choi, M. Kang, *Int. J. Hydrogen Energy*, 2007, **32**, 3841–3848.

49 L. Tang, R. Ji, X. Cao, J. Lin, H. Jiang, X. Li, K. S. Teng, C. M. Luk, S. Zeng, J. Hao, S. P. Lau, *ACS Nano*, 2012, **6**, 5102–5110.

50 M. Zhou, J. Bao, W. Bi, Y. Zeng, R. Zhu, M. Tao, Y. Xie, *ChemSusChem*, 2012, **5**, 1420–1425.

51 X. Qiu, M. Miyauchi, K. Sunada, M. Minoshima, M. Liu, Y. Lu, D. Li, Y. Shimodaira, Y. Hosogi, Y. Kuroda, K. Hashimoto, *ACS Nano*, 2012, **6**, 1609–1618.

52 X. Q. An, K. F. Li, and J. W. Tang, *ChemSusChem*, 2014, **7**, 1086–1093.

Graphical Abstract

The p-type Cu_2O/n-type TaON heterojunction nanorod array passivated with ultrathin carbon sheath as a surface protection layer is excellent in photoelectrochemical water splitting.